Emission spectrum of high-temperature (T = 2400 K) water vapor in the region 10650–10890 cm^{-1}

V.I. Serdyukov, L.N. Sinitsa, A.D. Bykov, L.N. Chebakova, and S.A. Tashkun

Institute of Atmospheric Optics,
Siberian Branch of the Russian Academy of Sciences, Tomsk

Received June 13, 2007

Emission spectra of the H_2O plasma near 0.9 μm were studied. Measurements were conducted using a grating spectrometer equipped with a linear photodiode array. Emission spectra were produced by a Multiplaz-2500 plasma source; the effective plasma temperature was 2400 K. The spectrum recorded has been assigned, and it was shown that nearly all lines in the observed spectrum belong to water vapor rotation-vibration transitions.

Introduction

Water vapor is one of the most important gaseous constituents of the atmosphere, it is responsible almost for 70% of the absorbed solar radiation and determines the global climate to a large extent. That is why the spectroscopic properties of water vapor are being under thorough scrutiny for a long time. The analysis of spectroscopic information includes the study of fine details of intramolecular dynamics, broadening and shift of spectral lines, weak transitions between high-excited states, as well as the compilation of extensive data banks.

New results in water vapor spectroscopy obtained in recent years are connected both with the fast development of experimental instrumentation and the theory of high-excited molecular states, for example, high-accuracy *ab initio* calculations taking into account nonadiabatic relativistic corrections to the potential energy function of the H_2O molecule.[1] In some publications (see, for example, Ref. 2), these results are considered as a breakthrough allowing a detailed pattern of the rotation-vibration energy spectrum up to the dissociation energy to be drawn.

Along with H_2O vapor spectra recorded at room temperature, high-temperature spectra of water vapor are intensively investigated, and the interest to them is caused by many reasons. Water vapor is found in many objects of the solar system, including Venus, Mars, and comets. Many H_2O spectral lines are observed in IR emission spectra of brown dwarf stars and red giant stars. A dense H_2O absorption spectrum (about 50 lines per 1 cm^{-1}) was recorded in the region of sunspots.[3] As a result, two atlases of sunspot absorption lines were published, and many strong lines among them were assigned to water vapor.[4]

Emission spectroscopy gives the qualitatively new information about weak water vapor lines. Water vapor emission spectra are used for monitoring, detection, and explanation of burning processes. For example, the aircraft-borne high-resolution Fourier spectrometer was used to record emission spectra of forest fires, and the emission lines of water vapor served to control the burning processes.[5]

Weak H_2O lines, especially, at long paths are significant contributors to the atmospheric absorption. To take them into account and determine their spectroscopic parameters, high-sensitive spectral devices are needed. High-temperature spectra enable one to obtain additional, more accurate information about parameters of weak absorption lines with high values of the rotational quantum number J.

Earlier, the emission spectra were studied in detail in the microwave, far- and near-IR spectral regions, and vibrational bands in the corresponding regions were analyzed. In the Visible, emission spectra remain poorly studied because of the small value of the Planck function in this region and corresponding low line intensity. In this paper, we have recorded and analyzed the emission spectrum of water vapor in the region 10650–10890 cm^{-1} at T = 2400 K. A plasmotron was used as a source of radiation.

1. Experiment

Water vapor is a plasma forming medium in a Multiplaz-2500 plasmotron. The vapor is generated from water closed in a sealed volume inside the plasmotron. Water, heated by the energy emitted by an electric arc, transforms into vapor and passes through the electric arc ($T \sim 8000$ K), dissociating into oxygen and hydrogen. The water dissociation starts at 1500 K, and at 4000 K the major part of water mass is already dissociating. Having passed through a nozzle of 1–2 mm in diameter, the gases, heated up to a high temperature, then were connected again, forming H_2O molecules, OH radical, oxygen, and hydrogen. The plasmotron is nearly similar to the oxygen–hydrogen flame. However, due to design features, the temperature of the observed flame significantly exceeds the temperature typical of the oxygen–hydrogen flame.

0235-6880/07/09 720-06 $02.00

Let us make a note relative to the dissociation of water vapor molecules at the increasing temperature. It is believed that water vapor molecules completely dissociate at a temperature higher 4000 K. Nevertheless, the water vapor molecules exist at such temperatures, but their number is very small due to short lifetime. Therefore, we can state that at high temperature the relative number of molecules in a static cell can be much lower than in a dynamic blown-through cell. In the jet leaving the plasmotron nozzle (an analog of a dynamic cell), permanent regeneration of the vanishing water vapor molecules takes place, and their concentration should be sufficient for reliable recording of water vapor emission spectra in the near IR.

To record the water vapor emission spectra, we have modernized a DFS-452 grating spectrometer with a hologram grating of 1200 mm^{-1} having dimensions of 60×50×10 mm and operating in the first order spectrum. For recording, we used a photodetector based on a linear CCD array and developed in the Laboratory of Molecular Spectroscopy of IAO.[6] The measured width of the spectrometer instrumental function was 0.1 cm^{-1}. The error in measurement of line positions was 0.02 cm^{-1}. The frequency scale was constructed using the emission spectra of a He–Ne gas-discharge tube.[7]

The useful signal was additionally increased by a cylindrical lens placed in front of the linear CCD array. Figure 1 shows the schematic view of the emission spectra recording. Such a system allows spectra to be recorded at different flame temperatures. The flame temperature was estimated from the rotational dependence of the emission intensity distribution of the OH radical.[7] The photodetector technical characteristics and the gas high temperature have allowed the reliable recording in the region 9500–12000 cm^{-1} of the emission spectrum of molecules contained in the flame.

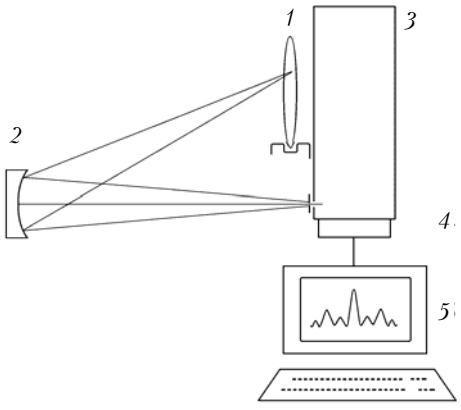

Fig. 1. Schematic view of the emission spectra recording: emitting gas *1*; mirror *2*; DFS-452 grating spectrometer *3*; photodetector based on a linear CCD array *4*; computer *5*.

2. Analysis of the spectrum

The plasmotron is a powerful source of plasma, in which the translational (gas) temperature achieves high values ($T \sim 10^4$ K). Therefore, it should be expected that water dissociates into OH and H in the dense region of plasma. In regions with less density and temperature, the recombination takes place followed by formation of H_2O molecules in different vibrational states. The spectrometer recorded the emission at different distances from the nozzle in the less heated region of the jet.

It should be noted that, in contrast to other investigations of high-temperature water vapor spectra, in which the hydrocarbon flame was used (methane–air mixture, acetylene torch) with a carbon dioxide gas as one of the burning products, no lines of foreign gases (CO_2, CO, or others) were in this work. The main product of the plasmotron was high-temperature water vapor, as well as OH radicals, OH^+, and OH^- ions connected with the H_2O molecule. Note that similar results can be also obtained with the use of the hydrogen–oxygen flame, whose the only product is water vapor as well.

The spectrum was analyzed based on the earlier developed software package.[8] We used the results of the high-accuracy variational calculation of energy levels and wave functions[1] and the H_2O spectrum calculated[9] using *ab initio* surface of the dipole moment function.

The following calculation technique was used. The line intensity was determined from the well-known equation

$$S_{if} = \frac{8\pi^3}{3hc} N g_i \eta_i \left[1 - \exp\left(-hc\nu_{if}/kT\right)\right] M_{if}, \qquad (1)$$

where

$$M_{if} = \left|\langle \psi_i | M_Z | \psi_f \rangle\right|^2 \qquad (2)$$

is the transition moment; ψ_i and ψ_f are the wave functions of the initial and final states of the transition under consideration; ν_{if} is the transition frequency; T is the temperature; N is the density; M_Z is the Z-projection of the transition dipole moment in the spatial coordinate system; η_i is the population of the state i; c is the speed of light; h is the Planck's constant; k is the Boltzmann constant; g_i is the degree of the level degeneration; E_i is the energy of the lower state.

For a medium in the equilibrium state

$$\eta_i = \frac{1}{Z(T)} \exp(-hcE_i / kT). \qquad (3)$$

The measured value is proportional to the radiation intensity

$$I(\nu) = I_0(\nu) \exp\left(-K(\nu) P L_{eff}\right). \qquad (4)$$

Here P is the pressure of the emitting gas; L_{eff} is some effective thickness of the emitting layer. The emission coefficient can be represented in the form

$$K(\nu) = S_{if} f(\nu), \qquad (5)$$

where $f(\nu)$ is the profile shape (Lorentzian in our calculation). To take into account the distorting influence of the spectral device, the instrumental

function was taken into account, and the measured signal was calculated as

$$I^*(\nu) = \int_{-\infty}^{\infty} A(\nu - \nu')I(\nu')\,d\nu'. \qquad (6)$$

To calculate the spectrum, we used the instrumental function with a width of 0.1 cm^{-1} corresponding to the spectrometer spectral resolution. The previous analysis has shown that the relationship between intensities of individual rotational-vibrational lines roughly corresponds to $T \approx 2400$ K, and all further calculations were performed for this temperature.

The results of calculations in comparison with the measured data are tabulated below and shown, as an example, in Fig. 2.

Table 1

Line position, cm^{-1}	Rel. intensity	Line position (calc.), cm^{-1}	V_1'	V_2'	V_3'	J'	K_a'	K_c'	J''	K_a''	K_c''	V_1''	V_2''	V_3''
1	2	3	4	5	6	7	8	9	10	11	12	13	14	15
10658.100	0.09													
10660.428	0.09	10660.66	3	1	0	8	0	8	7	1	7	0	1	0
10661.870	0.10	10662.06	3	1	0	8	0	8	7	1	7	0	1	0
10662.868	0.04	10662.86	0	2	2	8	2	7	8	1	8	0	0	0
10663.978	0.09	10664.09	3	0	0	9	4	6	9	5	5	0	0	0
10664.977	0.03	10665.04	2	1	1	7	4	3	6	4	2	0	1	0
10666.309	0.05													
10667.531	0.13	10667.76	1	4	0	12	5	8	11	2	9	0	0	0
10669.976	0.07	10670.15	2	0	1	3	2	2	2	2	1	0	0	0
10670.754	0.04	10670.85	0	7	0	10	3	8	9	6	3	0	0	0
10672.311	0.08	10672.28	2	1	1	7	2	6	6	2	5	0	1	0
10673.424	0.12	10673.55	2	0	1	3	0	3	2	0	2	0	0	0
10674.648	0.16	10674.61	2	1	1	8	0	8	7	0	7	0	1	0
10676.652	0.09	10676.79	0	0	3	11	3	9	12	3	10	0	0	0
10678.768	0.08	10678.59	0	7	0	13	2	12	12	3	9	0	0	0
10680.106	0.13	10680.10	2	2	0	9	7	3	9	6	4	0	0	0
10682.335	0.16	10682.36	0	2	2	10	5	5	9	6	4	0	0	0
10683.562	0.16	10683.72	2	0	1	4	3	1	3	3	0	0	0	0
10685.348	0.05	10685.27	2	1	1	8	4	4	7	4	3	0	1	0
10687.358	0.16	10687.40	2	0	1	4	0	4	3	0	3	0	0	0
10688.139	0.08	10688.25	2	0	1	4	2	3	3	2	2	0	0	0
10689.927	0.17	10690.04	2	1	1	10	0	10	9	0	9	0	1	0
10690.933	0.12	10691.04	2	0	1	10	7	3	9	7	2	0	0	0
10691.827	0.13	10691.77	2	0	1	6	5	1	5	5	0	0	0	0
10693.057	0.15	10693.09	2	1	1	9	4	6	8	4	5	0	1	0
10694.064	0.08	10694.07	2	0	1	7	6	2	6	6	1	0	0	0
10695.743	0.07	10695.90	1	2	1	5	4	2	4	2	3	0	0	0
10697.422	0.24	10697.36	3	0	0	10	2	8	10	3	7	0	0	0
10698.878	0.21	10698.97	2	0	1	4	2	2	3	2	1	0	0	0
10699.550	0.15	10699.58	2	0	1	9	6	3	10	2	8	0	0	0
10700.671	0.25	10700.68	2	0	1	4	1	3	3	1	2	0	0	0
10702.576	0.15	10702.68	2	1	1	12	1	12	11	1	11	0	1	0
10703.361	0.08	10703.44	2	1	1	11	2	10	10	2	9	0	1	0
10704.371	0.20	10704.43	2	0	1	5	2	4	4	2	3	0	0	0
10705.381	0.11	10705.51	2	0	1	5	3	2	4	3	1	0	0	0
10706.503	0.20	10706.41	0	3	2	6	3	3	5	2	4	0	1	0
		10706.87	1	2	1	11	6	5	11	4	8	0	0	0
10707.401	0.17	10707.58	2	1	1	13	1	13	12	1	12	0	1	0
10708.187	0.16	10708.21	2	0	1	6	4	2	5	4	1	0	0	0
10710.096	0.26	10710.05	2	0	1	6	1	6	5	1	5	0	0	0
10711.108	0.37	10711.02	0	0	3	11	4	7	11	6	6	0	0	0
10712.232	0.11	10712.23	1	3	1	10	3	7	9	1	8	0	1	0
10714.031	0.23	10713.48	3	0	0	5	2	4	4	1	3	0	0	0
		10714.04	3	0	0	7	1	6	6	2	5	0	0	0
10715.493	0.22	10715.42	3	1	0	5	0	5	5	1	4	0	1	0
10716.506	0.15	10716.65	3	0	0	8	1	8	7	0	7	0	0	0
10717.631	0.15	10717.83	2	0	1	6	2	5	5	2	4	0	0	0
10719.207	0.11													
10720.221	0.24	10720.23	2	0	1	7	1	7	6	1	6	0	0	0
10721.010	0.21	10721.17	2	0	1	12	7	5	11	7	4	0	0	0
10721.686	0.19	10721.87	2	0	1	7	0	7	6	0	6	0	0	0
10722.925	0.15	10723.01	1	2	1	7	3	5	6	1	6	0	0	0
10723.715	0.24	10723.75	2	2	0	8	3	6	7	0	7	0	0	0
10725.857	0.33	10725.76	3	0	0	7	2	6	6	1	5	0	0	0

Table 1 (continued)

1	2	3	4	5	6	7	8	9	10	11	12	13	14	15
10727.663	0.28	10727.76	2	2	0	6	6	1	5	5	0	0	0	0
10730.260	0.42	10730.16	0	2	2	10	5	6	10	4	7	0	0	0
10731.050	0.35	10731.01	2	0	1	8	0	8	7	0	7	0	0	0
10732.180	0.28	10732.26	2	0	1	7	3	5	6	3	4	0	0	0
10734.214	0.09													
10734.893	0.10	10734.78	0	2	2	13	6	8	12	7	5	0	0	0
10736.137	0.14	10736.02	3	0	0	9	2	8	8	1	7	0	0	0
10737.268	0.07													
10738.739	0.33	10738.83	2	0	1	6	2	4	5	2	3	0	0	0
10740.437	0.55	10740.28	3	0	0	11	1	11	10	0	10	0	0	0
10742.590	0.12	10742.48	0	0	3	12	1	12	12	1	11	0	0	0
10743.156	0.10	10743.22	0	2	2	14	5	10	13	6	7	0	0	0
10744.289	0.13	10744.37	2	0	1	14	1	13	14	1	14	0	0	0
10745.310	0.25	10745.23	0	2	2	12	2	11	11	1	10	0	0	0
10747.464	0.25	10747.52	2	0	1	8	4	4	7	4	3	0	0	0
10748.599	0.48	10748.52	2	0	1	10	1	10	9	1	9	0	0	0
10751.891	0.26	10751.77	2	0	1	9	4	6	8	4	5	0	0	0
10753.709	0.12	10753.77	3	0	0	12	2	11	11	1	10	0	0	0
10755.413	0.62	10755.47	0	1	3	7	1	6	8	1	7	0	1	0
10757.688	0.47	10757.68	2	0	1	10	1	9	9	1	8	0	0	0
10759.622	0.33	10759.56	2	0	1	10	5	5	9	5	4	0	0	0
10761.443	0.51	10761.52	2	0	1	12	1	12	11	1	11	0	0	0
10762.581	0.38	10762.56	2	0	1	11	2	10	10	2	9	0	0	0
10763.379	0.29	10763.17	3	0	0	4	4	0	3	3	1	0	0	0
10766.341	0.64	10766.46	2	0	1	13	1	13	12	1	12	0	0	0
10767.139	0.47	10767.15	0	0	3	10	1	10	11	1	11	0	0	0
10767.937	0.46	10767.95	2	0	1	12	1	11	11	1	10	0	0	0
10770.333	0.75	10770.76	3	0	0	5	4	2	6	3	3	0	0	0
10771.817	0.49	10772.06	0	8	0	15	0	15	14	3	12	0	0	0
10773.072	0.53													
10773.986	0.40	10773.78	2	0	1	11	8	3	11	6	6	0	0	0
10775.585	0.82	10775.73	2	0	1	7	4	3	7	2	6	0	0	0
10777.299	0.45	10777.29	2	0	1	12	2	10	11	2	9	0	0	0
10778.786	0.44	10778.57	2	0	1	13	2	11	12	2	10	0	0	0
10780.501	0.29	10780.78	2	0	1	15	1	14	14	1	13	0	0	0
10781.989	0.32	10781.84	2	0	1	13	4	10	12	4	9	0	0	0
10784.049	0.13	10784.15	2	0	1	15	0	15	14	0	14	0	0	0
10785.653	0.31	10785.59	3	0	0	13	4	10	12	3	9	0	0	0
10786.569	0.09	10786.72	2	0	1	17	0	17	16	0	16	0	0	0
10788.861	0.28	10788.92	2	0	1	10	3	7	9	3	6	0	0	0
10789.893	0.17	10789.73	3	0	0	12	4	9	11	3	8	0	0	0
10790.581	0.19													
10792.072	0.14													
10794.483	0.22	10794.74	2	0	1	14	3	11	13	3	10	0	0	0
10796.205	0.08	10796.21	0	0	3	9	9	0	9	9	1	0	0	0
10797.239	0.09	10797.26	3	0	0	6	4	3	5	3	2	0	0	0
10798.733	0.13	10798.83	2	0	1	13	3	10	12	3	9	0	0	0
10799.882	0.14	10799.95	2	0	1	11	4	7	10	4	6	0	0	0
10801.837	0.07	10801.83	0	0	3	6	4	2	7	4	3	0	0	0
10803.562	0.16	10803.58	2	0	1	12	3	9	11	3	8	0	0	0
10805.404	0.05													
10806.670	0.05	10806.73	2	0	1	11	5	6	11	3	9	0	0	0
10808.743	0.22	10808.84	2	0	1	12	4	8	11	4	7	0	0	0
10810.818	0.15	10811.01	3	0	0	4	4	0	5	3	3	0	0	0
10812.317	0.11	10812.19	3	0	0	1	0	1	2	1	2	0	0	0
10813.008	0.11	10812.99	2	0	1	13	4	9	12	4	8	0	0	0
10814.623	0.08	10814.53	0	0	3	11	8	4	11	8	3	0	0	0
10816.124	0.08	10816.18	0	0	3	6	3	3	7	3	4	0	0	0
10816.932	0.08	10816.89	1	2	1	8	5	3	7	3	4	0	0	0
10818.086	0.15	10818.01	2	0	1	14	5	9	13	5	8	0	0	0
10819.472	0.08	10819.70	0	0	3	10	2	8	10	4	7	0	0	0
10820.743	0.18	10820.60	2	2	0	14	6	9	13	5	8	0	0	0
10822.708	0.09	10822.78	2	0	1	10	10	1	10	8	2	0	0	0
10824.443	0.15													
10825.831	0.10	10825.67	3	0	0	3	0	3	3	1	2	0	0	0
10828.030	0.09	10828.10	0	0	3	6	2	4	7	2	5	0	0	0

Table 1 (continued)

1	2	3	4	5	6	7	8	9	10	11	12	13	14	15
10829.535	0.11	10829.62	3	0	0	3	3	0	4	2	3	0	0	0
10830.693	0.10	10830.67	0	0	3	5	4	2	6	4	3	0	0	0
10832.431	0.12	10832.40	0	0	3	9	8	2	9	8	1	0	0	0
10833.706	0.13													
10835.213	0.13	10834.98	0	2	2	7	4	4	6	3	3	0	0	0
10836.953	0.09	10837.12	2	0	1	6	3	3	5	1	4	0	0	0
10838.694	0.09	10838.59	0	2	2	11	8	3	11	7	4	0	0	0
10839.506	0.09													
10840.551	0.12	10840.56	0	0	3	8	8	1	8	8	0	0	0	0
10841.248	0.10	10841.53	3	1	0	4	2	2	4	1	3	0	1	0
10842.061	0.09													
10843.339	0.11	10843.48	0	0	3	4	2	2	4	4	1	0	0	0
10844.850	0.13	10844.67	3	0	0	9	7	3	8	6	2	0	0	0
10846.361	0.20	10846.34	0	0	3	7	1	7	8	1	8	0	0	0
10848.339	0.11	10848.77	0	1	3	3	2	1	4	2	2	0	1	0
10849.153	0.12	10849.30	3	1	0	1	1	1	0	0	0	0	1	0
10851.481	0.16	10851.49	0	0	3	5	3	3	6	3	4	0	0	0
10852.180	0.15	10852.40	0	2	2	9	8	1	9	7	2	0	0	0
10855.791	0.16	10856.05	0	1	3	8	5	3	8	5	4	0	1	0
10857.773	0.17	10857.66	3	0	0	12	5	8	11	4	7	0	0	0
10858.473	0.15	10858.43	0	0	3	11	7	5	11	7	4	0	0	0
10859.289	0.16	10859.41	0	1	3	3	1	2	4	1	3	0	1	0
10861.156	0.16	10861.03	0	1	3	7	5	3	7	5	2	0	1	0
10862.674	0.16	10862.93	2	1	1	8	3	5	7	1	6	0	1	0
10863.608	0.17	10864.14	0	0	3	10	7	3	10	7	4	0	0	0
10865.477	0.18	10865.90	3	0	0	9	5	4	8	4	5	0	0	0
10866.996	0.21	10866.69	0	1	3	6	5	2	6	5	1	0	1	0
10867.814	0.20	10867.65	2	0	1	7	3	4	6	1	5	0	0	0
10869.684	0.24	10869.64	3	0	0	11	4	7	11	3	8	0	0	0
10871.439	0.30	10871.33	3	0	0	12	9	3	11	8	4	0	0	0
10874.365	0.24	10874.30	3	0	0	9	4	5	9	3	6	0	0	0
10875.536	0.30	10875.55	0	0	3	8	7	1	8	7	2	0	0	0
10876.473	0.24	10876.53	2	0	1	5	4	2	4	2	3	0	0	0
10877.410	0.24	10877.26	3	0	0	8	4	4	7	5	3	0	0	0
10879.285	0.27	10879.25	0	1	3	3	0	3	4	0	4	0	1	0
10880.223	0.25	10880.27	3	1	0	6	4	3	6	3	4	0	1	0
10881.630	0.33	10881.56	0	0	3	7	7	0	7	7	1	0	0	0
10883.038	0.26	10883.10	3	0	0	12	6	7	12	5	8	0	0	0
10884.915	0.32	10885.08	0	0	3	4	2	2	5	2	3	0	0	0
10885.972	0.34													
10887.146	0.31													
10888.790	0.32	10888.68	0	0	3	10	4	6	11	2	9	0	0	0
10889.613	0.33	10889.60	3	0	0	8	3	5	7	2	6	0	0	0
10890.906	0.35	10891.08	3	0	0	6	3	3	6	2	4	0	0	0

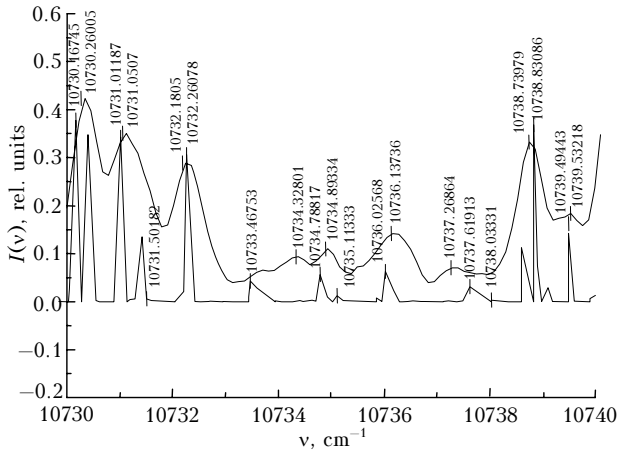

Fig. 2. An interval of water vapor emission spectrum: experiment (top curve) and calculation (bottom curve).

Lines in the plasma emission spectrum were assigned by a simple comparison of the calculated and experimental spectra, as well as the data from Ref. 10. Since the accuracy of the variational calculation is quite high and the calculation error is on the average 1 cm^{-1}, line intensities within several reciprocal centimeters were compared. The analysis of correlation between intensities of close line groups allowed rather reliable assignment of the observed peaks in the recorded spectrum to some or other quantum transitions in the molecule. The results of assignment are presented in columns 4–15 of the Table as vibrational quantum numbers V'_1, V'_2, V'_3 rotational quantum numbers J', K'_a, K'_c of the upper state, as well as rotational and vibrational quantum numbers J'', K''_a, K''_c, V''_1, V''_2, V''_3 of the transition lower state.

The spectrum includes lines determined by transitions from high rotational levels with the rotational quantum number up to $J = 17$, as well as lines of hot bands because of the high temperature of water vapor under study.

Conclusions

The results of analysis of the emission spectrum of H_2O plasma produced in high-power arc discharge have shown that nearly all lines in the observed spectrum can be assigned to rotation-vibration transitions of the water vapor molecule. Some hot transitions and transitions to high bending states are also observed. The effective temperature of plasma is about 2400 K.

Acknowledgements

This work was supported in part by the Russian Foundation for Basic Research (Grant No. 05–03–32782) and the RAS Program "Optical Spectroscopy and Frequency Standards."

References

1. H. Partridge and D. Schwenke, J. Chem. Phys. **106**, No. 11, 4618–4639 (1997).
2. J. Tennyson, M.A. Kostin, P. Barletta, G.J. Harris, O.L. Polyansky, J. Ramanlal, and N.F. Zobov, Comput. Phys. Commun. **163**, No. 2, 85–116 (2004).
3. L. Wallace, P. Bernath, W. Livingston, K. Hinkle, J. Busler, B. Guo, and K.-Q. Zhang, Science **268**, 1155–1158 (1995).
4. L. Wallace, W. Livingston, K. Hinkle, and P.F. Bernath, Astrophys. J. Suppl. **106**, 165–169 (1996).
5. H. Worden, R. Beer, and C.P. Rinsland, J. Geophys. Res. **102**, 1287–1299 (1997).
6. Yu.A. Poplavskii, V.I. Serdyukov, L.N. Sinitsa, A.P. Shcherbakov, and Yu.A. Matul'yan, Nauka – Proizvodstvu, No. 9, 28–29 (2003).
7. S.N. Mikhailenko, G.Ch. Mellau, E.N. Starikova, S.A. Tashkun, and Vl.G. Tyuterev, J. Mol. Spectrosc. **233**, No. 1, 32–59 (2005).
8. A.D. Bykov, O.V. Naumenko, A.M. Pshenichnikov, L.N. Sinitsa, and A.P. Shcherbakov, Opt. Spectrosc. **94**, No. 4, 528–537 (2003).
9. http:/ iao.ru.spectra
10. L.S. Rothman, A. Barbe, D.C. Benner, L.R. Brown, C. Camy-Peyret, M.R. Carleer, K. Chance, C. Clerbaux, V. Dana, V.M. Devi, et al., J. Quant. Spectrosc. Radiat. Transfer **82**, No. 1, 5–44 (2003).